J. Mater. Environ. Sci. 6 (12) (2015) 3388-3394
ISSN : 2028-2508
CODEN: JMESCN

Synthesis, crystal structure and vibrational spectroscopy studies of the lacunar apatite $NaPb_2Ca_2(PO_4)_3$

A. Chari[1], B. Orayech[2], A. Faik[2], J. M. Igartua[3], A. El Bouari[1*]

[1]*Laboratoire de Physico-Chimie des Matériaux Appliqués (LPCMA), Faculté des Sciences Ben M'Sik ,Casablanca, Université Hassan II de Casablanca, Maroc*
[2]*CICenergigune, Albert Einstein 48, 01510 Miñano, Alava, Spain*
[3]*Fisika Aplikatua II Saila, Zientzia eta Teknologia Fakultatea, UPV/EHU, P.O. Box 644, 48080 Bilbao, Spain.*
[*]*Corresponding Author. E-mail: elbouari@gmail.com; Tel: (+212662124075)*

Abstract
Powder $NaPb_2Ca_2(PO_4)_3$ lacunar apatite was synthesized by the solid-state reaction method, and its crystal structure was investigated by Rietveld analysis. $NaPb_2Ca_2(PO_4)_3$ material is hexagonal apatite at room temperature, adopting the space group $P6_3/m$ (ITA No. 176), a=b=9.6075(2)Å, c=7.0167(1)Å, Z=2. Rietveld refinements showed that the site 4f is shared by three cations Ca, Pb and Na; while, the 6h is occupied by the Pb and Na cations. The structure can be described as built up from the PO_4tetrahedra and the sixfold coordination cavities, which delimit hexagonal tunnels along the c-axis direction. These tunnels are linked by the cations occupying the 4f sites. Raman spectroscopy analysis has been carried out. The observed frequencies were assigned and discussed on the basis of unit-cell group analysis and by comparison to other apatite-type materials.

Keywords: Lacunar apatite, X-Ray diffraction, Crystal structure, Raman spectroscopy.

Introduction
Compounds of the apatite type have been studied extensively in the literature. These materials can be used for various applications, such as catalysts [1], ionic exchangers for harmful ions [2] and luminescent materials [3,6,7] as well as in optoelectronics [8] and bio-materials [9]. They are also attracting considerable attention as a new class of oxide ion conductors [10,11,28-32]. The reference crystal is the calcium Fluorapatite $Ca_{10}(PO_4)_6F_2$ (with the general chemical formula $M_{10}(YO_4)_6X_2$) that crystallizes in the hexagonal system with the $P6_3/m$ space group [12,4,5].
The apatite structure is described as follows. The YO_4 tetrahedrons are arranged around the 63 screw axes forming columns around the crystallographic c axis with X ions on the axis [13]. In one cell, the ten cations are distributed on two sites where six of them fill the (6h) sites making equilateral triangles and the remaining four cations occupy the (4f) sites. The coordination number is seven for the (6h) cations, six O and one X; while is nine (Oxygen atoms) for the (4f) cations building trigonal tri-capped prisms stacked in columns in the [001] direction.
The so-called Lacunar Apatites, with lack of X anion and the general formula $APb_4(XO_4)_3$, (A= Li, Na, K, Ag), have already been widely studied. A large number of cations combinations were proposed by several authors. It is been shown that the cation Pb^{2+} have a crucial role by preserving the apatite's network, which is related to the presence of the electronic doublets $6s^2$ that compensate for the Coulomb imbalance due to the existence of the anion gap in the tunnels of the apatite structure [13,15,21].
Furthermore, Lead in apatite structure is of interest from two points of view. First, lead is known as a 'bone seeker' in that it accumulates in bones and teeth, second, it may contribute to deviation from the general formula of apatites. Because of the importance of these types of lacunar apatites and the problems that may cause in biomaterial applications, it seems to us of interest to perform the structural characterization, using X-ray diffraction and Raman spectroscopy, of the composition of lead calcium phosphates apatites of sodium without fluor anions $NaPb_2Ca_2(PO_4)_3$.

2. Experimental details

2.1. Sample preparation

$NaPb_2Ca_2(PO_4)_3$ sample was synthesized by conventional solid-state reaction. Stoichiometric ratios of Na_2CO_3(99.999%), $Pb(NO_3)_2$ (99.999%), $CaCO_3$(99.999%) and $(NH_4)_2HPO_4$ (99.98%) were mixed in acetone medium and ground in an agate mortar according to the following chemical reaction:

$$1/2Na_2CO_3 + 2Pb(NO_3)_2 + 2CaCO_3 + 3(NH_4)_2HPO_4 \longrightarrow NaPb_2Ca_2(PO_4)_3 + 5/2CO_2 + 10NH_3 + 53/2\ H_2O$$

The resulting residual powder was then ground and slowly calcined at 470 K for 24h, 870 K for 24h and 1170 K for 48h. The sample was later ground, pressed to pellet using a cold isostatic press and annealed in air at 1220 K for 24h. After each heating, the sample was cooled down slowly (20K/h) to ensure more complete absorption of oxygen by the lattice and reground to improve homogeneity. The obtained colour of the synthesized sample was white. X-ray diffraction measurements were performed after each heating in order to control the quality of the obtained material.

2.2. Diffraction measurements and data analysis

Room temperature X-ray powder diffraction analysis was accomplished with a STOE STADI-P diffractometer equipped with a focusing germanium primary monochromator and a linear position-sensitive detector (PSD). The $CuK_{\alpha 1}$=1.5406 Å wavelength was used. The data were collected in the range $20° < 2\theta < 120°$ with a step of 0.02° and a count-time of 600s per step.

The Rietveld refinement [16] of the structure was performed using FullProf. The peak shape was described by a pseudo-Voigt function convoluted with axial divergence asymmetry function. The background level was modeled using selected points. The refined parameters were: scale factor, zero shift, lattice constants, peak profile, asymmetry parameters, amplitudes of the modes transforming according to the irreps and independent isotropic atomic displacement parameters.

2.3. Raman spectroscopy

The Raman measurements were performed on Jobin Yvon T64000 spectrometer; coupled with an optical microscope (x100 objective) and a CCD detector in a backscattering geometry. The γ= 514.5 nm line was used as excitation source. Rejection of the elastic peak was achieved using a holographic notch filter, which resulted in a cutting of the scattered signal below 100 cm1. The laser power on the sample was maintained 3 at mW mm^{-2}. The acquisition time was 30 s (3 accumulations).

3. Results and discussion

The resulting X-ray powder diffraction (XRPD) pattern for $NaPb_2Ca_2(PO_4)_3$was performed by means of the computer program DICVOL [18]. The first 25 peak positions, with a maximal absolute error of 0.03°, were used as input data. The X-ray diffraction pattern was assigned to a hexagonal apatite structure.

The full pattern refinement was carried out by means of the Rietveld method using the Fullprof program [17] integrated in WINPLOTR software [16]. The atomic coordinates of $NaPb_3Ca(PO_4)_3$ with space group $P6_3/m$ were used as a starting model for Rietveld refinement. The refinement involved 26 atomic parameters (including positions, occupancies, and isotropic thermal displacements), and the occupancy factors of O and P were assumed as constant, in agreement with the apatite stoichiometry. The crystallographic characteristics and conditions for data collection are given in Table 1. The refinement leads to a rather good agreement between the experimental and calculated XRPD patterns. All the observed reflections could be indexed in the space group $P6_3/m$ (ITA No. 176) and the structural model indicators converged to R_{Bragg} = 0.89% and χ^2 = 1.32. The results show that the sample is free of impurities since no additional extra peaks were detected.

Figure 1 shows the Rietveld refinement patterns for $NaPb_2Ca_2(PO_4)_3$. The point symbols represent the observed diffraction pattern; the solid line represents the calculated pattern. The short vertical lines mark the position of possible Bragg reflection for the apatite compound. The resulting data for atomic coordinates and isotropic temperature factors are listed in Table 2. The interatomic bond distances and angles are given in Table 3.

Table 1: The crystallographic characteristics and XRPD data collection conditions for the $NaPb_2Ca_2(PO_4)_3$.

Diffractometer	STOE STADI-P
Radiation	$CuK_{\alpha 1}$=1.5406 Å
Angular range 2θ °	10-80°
Step scan increment 2θ °	0.02°
Count time (s/step)	300s
Space group	$P6_3/m$ (ITA No. 176)
Cell parameters (Å)	a=9.6075(1) and c=7.0167(1)
Volume (Å³), Z	V=560.904(3), Z=2
Number of refined parameters	26
Peak-shape parameters	U=0.0570(1), V=-0.0096(3) W=0.0154(4)
Peak shape	Pseudo-Voigt
Reliability factors	R_p= 1.57%, R_{wp}= 2.09% R_{exp}= 0.90%, χ^2= 1.32 R_{Bragg}= 0.89

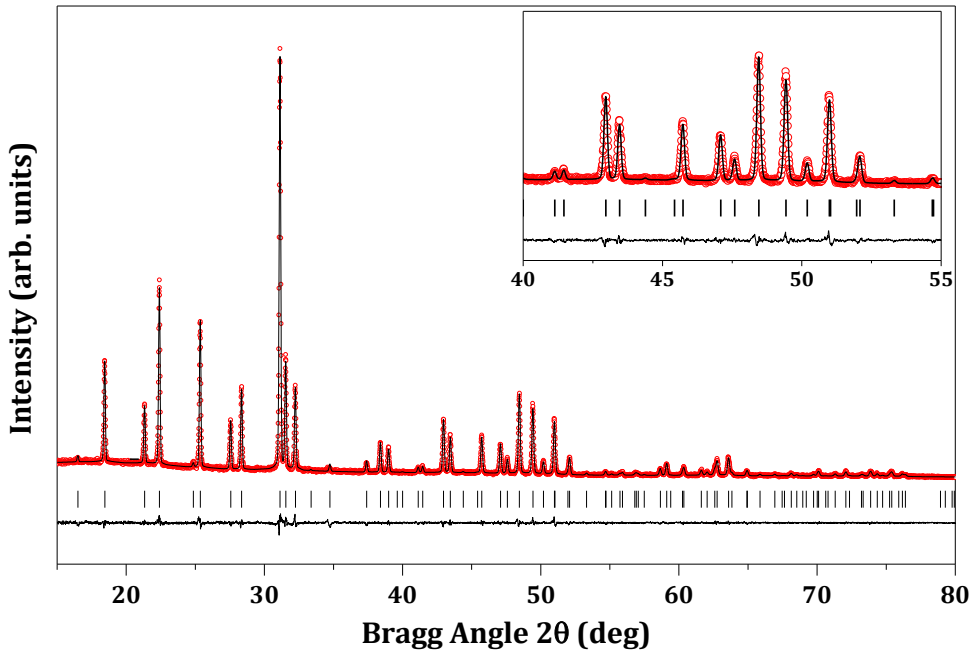

Figure 1: Experimental (symbols) and calculated (line) X-ray profiles for the Rietveld refinement of $NaPb_2Ca_2(PO_4)_3$ at room temperature using a structural model with $P6_3/m$ space group. The bars in the lower part of the graphics represent the Bragg peak positions. Inset shows in detail a selected 2θ region showing the goodness of the refinement.

Table 2: Crystal structure data and refinement results for $NaPb_2Ca_2(PO_4)_3$, in the space group $P6_3/m$ (ITA No. 176), from XRPD data.

Atom	Site	x	y	z	Biso(Å²)	Occupancy
Na1	4f	1/3	2/3	0.5021(2)	1.46(1)	0.47(1)
Pb1	4f	1/3	2/3	0.5021(2)	1.46(1)	0.02(1)
Ca1	4f	1/3	2/3	0.5021(2)	1.46(1)	0.51(1)
Pb2	6h	0.25451(2)	0.2522(2)	1/4	1.59(3)	0.83(2)
P1	6h	0.25451(2)	0.2522(2)	1/4	1.19(2)	1.00
O1	6h	0.49206(1)	0.3421(3)	3/4	1.78(3)	1.00
O2	6h	0.47176(3)	0.5852(1)	3/4	1.78(3)	1.00
O3	12i	0.26906(1)	0.3503(1)	0.5722(1)	1.78(3)	1.00

Figure 2a shows the projection of the $NaPb_2Ca_2(PO_4)_3$structure along the(001) direction. It shows the expected anion vacancy in the wider tunnel centered on the c axis, which has been already observed in the previous studied lacunary apatites. Figures 2b and 2c, show the polyhedra of the 6h and 4f site, respectively, and their connection with the adjacent PO_4 tetrahedra.
The analysis of the tetrahedra PO_4 revealed that the average P-O distance 1.552 Å was similar to the average values observed in mono-phosphates ions 1.54 Å [27]. On the other hand, the O-P-O angles were noted to vary between 105.21° and 107.31°, with an average value of 110.89°, which is a bit smaller than the one of a uniform tetrahedron 109.47°. This distortion of the PO_4 tetrahedra can be attributed to the substitution of Ca for Pb cation, which drastically changes both the electronic and the geometric environment of the PO_4 ions.

In the structure of $NaPb_2Ca_2(PO_4)_3$, there were two symmetrically non-equivalent sites 4f and 6h. The 4f site is occupied by Na^+, Ca^{2+} and Pb^{2+}. In this case the Lead is a minor component, where the Calcium is a major. Those cations are coordinated to nine oxygen anions belonging to six distinct tetrahedra. Each polyhedron was linked to three PO_4 tetrahedra via corners and to three other tetrahedra via edges. In the 4f site, the nine distances had an average value of 2.611(1) Å, which was slightly larger to the one of Fluoroapatite 2.56(2)Å [27], where the 4f was 100% occupied by Calcium. This variation could presumably be attributed to the fact that in the present studied material, the 4f is occupied by more cations whose ionic radii are bigger than Calcium (Ca^{2+}=1.18Å, Na^+=1.24Åand Pb^{2+}=1.35Å).
The 6h site, situated at the border of the larger section is occupied by $Na^{1+}$and Pb^{2+}. Those cations are inserted into six-fold sites that constituted the walls of the tunnels. Each polyhedron was linked to four PO_4 tetrahedra via corners and to one PO_4 via edge and one of the free oxygen O3. In this site, Lead imposes its weight and the average Na_2/Pb_2-O distance 2.601Å is similar to that in $NaPb_{4(}PO_4)_3$. The electron lone pair constitutes the seventh ligand of Lead in the 6h site, and plays the same role as the Y anions that normally fill the hexagonal tunnels in the defect-free apatites.

Table 3: Main bond distances (Å) and selected angles (°) for $NaPb_2Ca_2(PO_4)_3$ obtained from XRPD data using the space group $P6_3/m$ (ITA No. 176).

Na2/Pb2O$_6$ Octahedra	**Distance or angles**
Na2/Pb2-O3 * 2	2.426(3)
Na2/Pb2-O3* 2	2.572(1)
Na2/Pb2-O2	2.290(3)
Na2/Pb2-O1	3.110(3)
Average distance	**2.601(2)**
Na1/Ca1/Pb1O$_9$ Polyhedra	**distance**
Na1/Ca1/Pb1-O1_3	2.471(4)
Na1/Ca1/Pb1-O2_3	2.536(1)
Na1/Ca1/Pb1-O3_3	2.825(3)
Average distance	**2.611(1)**
PO$_4$ Tetrahedra	**1.543(2)**
P1-O1	1.567(1)
P1-O2	1.549(4)
P1-O3	1.549(4)
Average distance	**1.552(1)**
O1-P1-O2	105.21(2)
O1-P1-O3 * 2	116.52(1)
O2-P1-O3 * 2	106.24(1)
O3-P1-O3	107.31(2)

Table 4 shows the cell parameters reported by other authors for similar materials, together with the obtained cell parameters from the present work. These values are also plotted in Figure 3 againt the x value in the formula $NaPb_{4-x}Ca_x(PO_4)_3$. It is clearly shown that the progressive substitution of Lead by the Calcium provokes a decrease of the unit cell parameters a, c and V . This decrease is due to the substitution of Pb^{2+} (r_i=1.35 Å) by Ca^{2+}(r_i=1.18 Å). The linear decrease of the lattice parameters when Lead is replaced by calcium shows that Vegard law is verified. Similar linear evolution of the cell parameters was reported for other solid solutions of lacunar apatite materials [20,22,23], where a given proportion of Na where replaced by equal proportion of Ka. This behaviour was observed for the P, V and as apatite families.

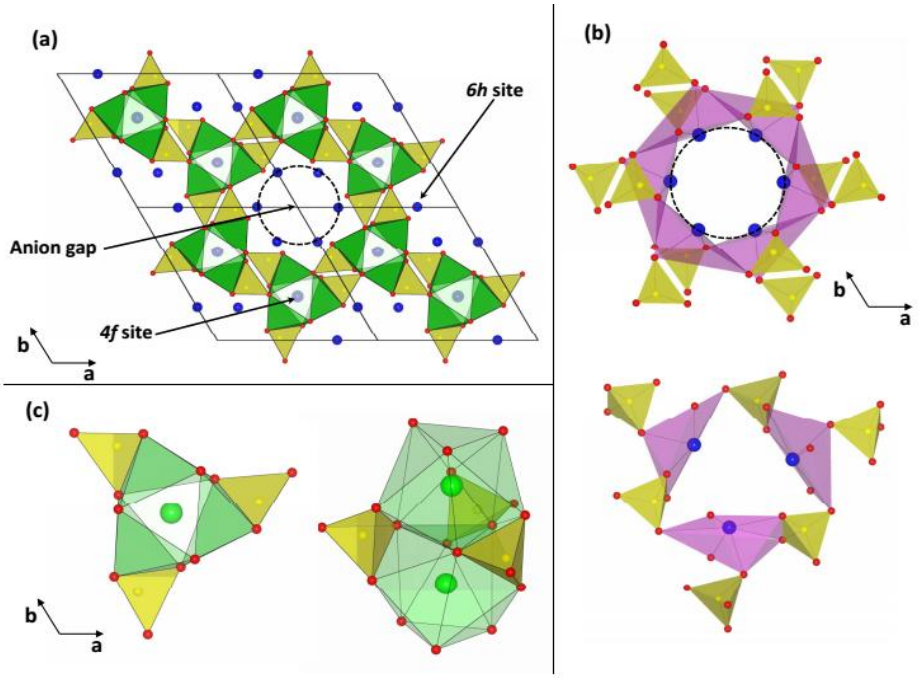

Figure 2: (a) Projection of the $NaPb_2Ca_2(PO_4)_3$ structure, along the (001) direction, showing in details the two sites 6h and 4f. In (b), the anionic tunnel is shows, which is surrounded by the 6h site occupying atoms (in blue). The (c) shows the polyhedral of the 4f atoms (in green), which are connected to each other by three oxygens and surrounded by the PO_4 tetrahedra (in yellow).

Table 4: Refined values of the cell parameters and volume of $NaPb_2Ca_2(PO_4)_3$using the space group $P6_3/m$ (ITA No. 176). The results are compared to the cell parameters and volumes of others lacunar-apatite materials, having as well the $P6_3/m$ space group. The [PW] stands for present work.

Cell Parameters a(Å)	a(Å)	c(Å)	V (Å³)	[Ref.]
$NaPb_4(PO_4)_3$	9.721(4)	7.186(5)	588.08(1)	[20]
$NaPb_4(PO_4)_3$	9.725(8)	7.190(1)	588.90(1)	[24]
$NaPb_3Ca(PO_4)_3$	9.658(8)	7.081(6)	572.00(2)	[25]
$NaPb_2Ca_2(PO_4)_3$	9.6075(1)	7.0167(1)	560.90(3)	[PW]

3.1 Spectroscopy Raman analysis

In order to get a better understanding of the material and to study the influence of the substituted ions on the vibrational modes of the Phosphate groups, the Raman spectra are analyzed. Factor group analysis of the $NaPb_2Ca_2(PO_4)_3$ hexagonal structure $P6_3/m$, shows that the normal modes of vibration can be classified among the irreducible representations of C_{6h} as the following equation:

$$\Gamma = 12A_g+8E_{1g}+12E_{2g}+8A_u+12B_u+8B_g+12E_{1u}+8E_{2u}.$$

Where the internal mode contribution of the PO_4 groups to the IR- and Raman-active vibration was :

$$\Gamma_{PO4} = 6A_g(\nu_1 + \nu_2 + 2\nu_3 + 2\nu_4)+3E_{1g}(\nu_2 + \nu_3 +\nu_4)+6E_{2g}(\nu_1+\nu_2+2\nu_3+2\nu_4)+6A_u(\nu_1+\nu_2+2\nu_3+2\nu_4)+3E_{1u}(\nu_2+\nu_3+\nu_4).$$

Where the g and u modes refer to Raman and IR-active vibrations, respectively. The Raman spectra are shown in Figure 4. The spectral data and proposed vibrational assignments are presented in the insets Figure 3a and 3b. As shown in Raman spectrum three families of lattice vibrations can be defined; Na/Ca/Pb-O, Na/Pb-O external and translational modes, and rotational modes of the PO_4 tetrahedra. These modes could be classified according to three regions: a pattern of bands was observed in the interval [350 to 500cm^{-1}] is attributed to the O-P-O bending vibrations where the bands related to $\nu_2$and ν_4 are located in [350 to 500 cm^{-1}] and [500 to 650 cm^{-1}], respectively. At higher frequency a series of bands observed in the interval [850 to 1100 cm^{-1}]is assigned to the P-O stretching modes. The two strong bands between 850 to 1000 cm^{-1} and the weaker ones observed interval 1000 to 1100 cm^{-1}canbe attributed to ν_1 and ν_3 of the PO_4 tetrahedra, respectively. The positions of these bands were similar to those reported previously by Toumi et al. [26] and for the Fluoroapatites [27].

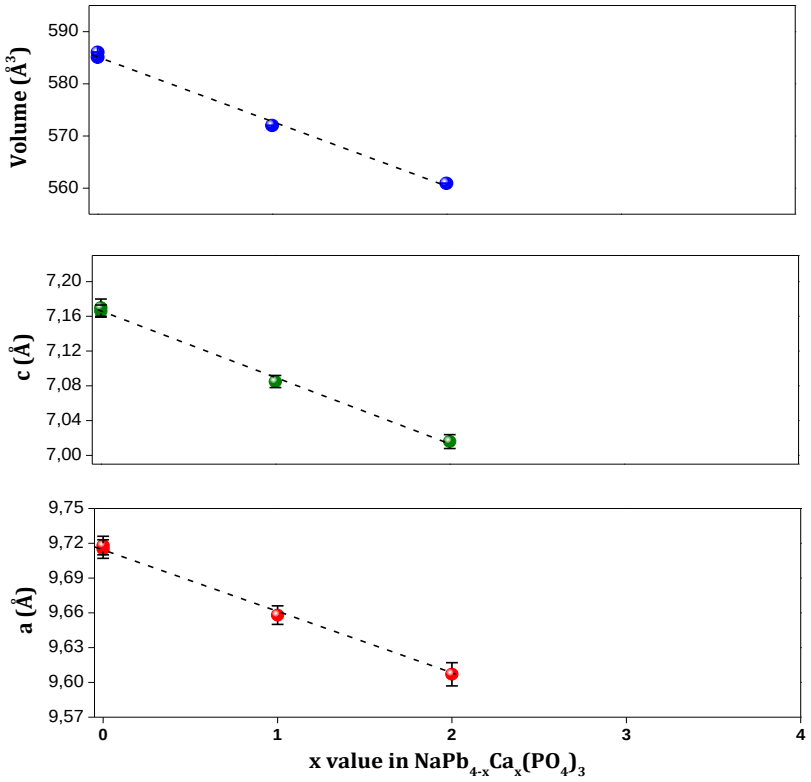

Figure 3: Cell parameters evolution according to the x value in the formula$NaPb_{4-x}Ca_x(PO_4)_3$, which represents the number of substituted Lead atoms. The linear evolution of the lattice parameters confirms that Vegard law is verified. The dashed lines are guide for the eye.

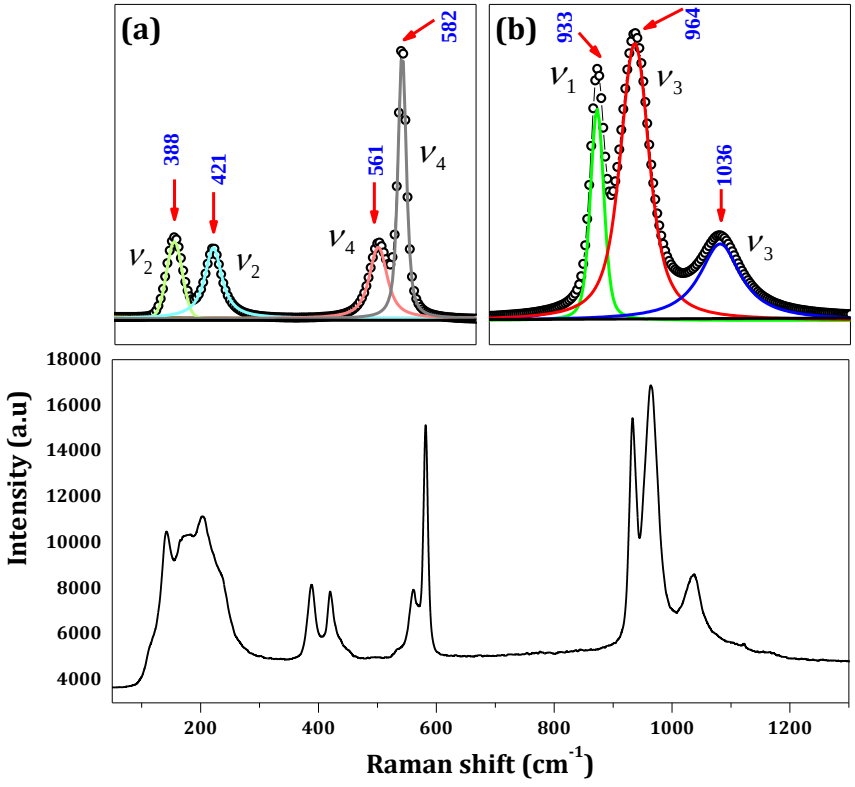

Figure 4: Experimental Raman spectrum of $NaPb_2Ca_2(PO_4)_3$ and best fit using the causal Voigt model. The insets (a) and (b) show the fitting of the two regions [350 to 650 cm^{-1}] and [850 to 1100 cm^{-1}] related to $\nu_2 + \nu_4$ and $\nu_1 + \nu_3$, respectively.

Conclusion

The $NaPb_2Ca_2(PO_4)_3$ lacunar apatite was successfully synthesized by the solid-state reaction method and characterized by X-ray diffraction and Raman spectroscopy. Its structure have been determined by Rietveld, adopting the space group $P6_3/m$ (ITA No. 176), with a=b=9.6075(2)Å and c=7.0167(1)Å The analysis shows that the site 4f is shared by three cations Ca, Pb and Na.While the 6h is occupied by the Pb and Na cations. The apatite contained channels where oxygen ions were located in the 2a sites. The analysis of data from vibrational spectroscopy provided support for the symmetry $P6_3/m$.

References

1. Matsumura Y., Sugiyama S., Hayashi H., Moat J. B., *J. Solid State Chem.* 114 (1995) 138.
2. Suzuki T., *Gypsum. Lime* 204 (1986) 314.
3. Smet B. M. J., *Mater. Chem. Phys.* 16 (1987) 283.
4. Sahoo P. P., Payne J. L., Li M., Claridge J. B., Rosseinsky M. J., *Journal of Physics and Chemistry of Solids* (2015) 82-87.
5. Mokoena P.P., Nagpure I.M., Kumar V., Kroo R. E., Olivier E.J., Neethling J. H., Swart H. C., Ntwaeaborw O.M., *Journal of Physics and Chemistry of Solids* (2014) 998-1003.
6. Blasse G., *Mater. Chem. Phys*. 16 (1987) 201.
7. Tachihante M., Zanbon D., Cousseins J. C., *Eur .J . Solid State Inorg. Chem.* 33 (1996) 713.
8. Deloach L. D., Payne S. A., Smith L. K., Kway W.L., Krupke W.F., *J. Opt. Soc. Am B : Opt. Phys.* 11 (1994) 269-276.
9. Ohtsuki C., Kokubo T., Yamamuro T., *Non-Cryst J.. Solids* 143 (1992) 8492.
10. Leon-Reina L., Martin-Sedeno M. E., Losilla E. R., Caberza A., Martinez- Lara M., Bruque S., Marques F. M. B., Sheptvakov D. V., Aranda M. A. G., *Chem. Mater.* 15 (2003) 2099.
11. Wenhui Y., Rongping S., Li L., Chin. *J. Chem. Eng.* 18 (2010) 328-332.
12. Naray-Szabo S., *Z. Kristallogr.* 75 (1930) 323.
13. El Koumiri M., Oishi S., Sato S., El Ammari L., Elouadi B.. *Mater. Res. Bull.* 35 (2000), 503.
14. Quarton M., Oumba M.T., Freundlich W., Kolsi. A.W. *Mater. Res. Bull*, 19 (1984), 1063
15. Ternane R., Frid M., Kbir-Ariguib N., Trabelsi-Ayedi M. *J. Alloys Compd*., 308 (2000), 83.
16. Rietveld H. M., *J. Appl. Crystallogr*. 2 (1969) 65.
17. Rodriguez-Carvajal J., *Physica B* 192 (1993) 55.
18. Boultif A., Louer D., *J. Appl. Crystallogr.* 24 (1991) 987.
19. Mathew M., Brown W. E., Austin M., Negas T., *J. Solid. Stat. Chem.* 35 (1980) 69-76.
20. Azrour M, et al. *Journal of Physics and Chemistry of Solids*. 72 (2011) 1199-1205.
21. Guerra-Lopez J. R., Echeverra G. A., Guida J. A., Vina R., Punte G., *J. Phys. Chem. Sol*. 81 (2015) 57-65.
22. Azdouz M., et al. *J. of Molecular Structure* 963 (2010) 258-266.
23. Manoun B. et al., *J. of Molecular Structure* 986 (2011) 1-9.
24. El Koumiri M. et al. *Materials Research Bulletin* 35 (2000) 503-513.
25. Naddari T., El Feki H., Savariault J. M., Salles P., Ben Salah A., *Solid State Ionics* 158 (2003) 157-166.
26. Toumi M., Mhiri T., *Mater. Res. Bull.* 43 (2008) 1346-1354.
27. Toumi M., Smiri-Dogguy L., Bulou A., *J. Solid State Chem*. 149 (2000) 308-313.
28. Essehli R., Belharouak I., Ben Yahia H., Maher K., Abouimrane A., Orayech B., Calder S., Zhou X. L., Zhou Z. and Sun Y-K., *Dalton Trans*. 44 (2015) 7881-7886
29. Essehli R., Belharouak I., Ben Yahia H., Chamoun R., Orayech B., El Bali B., Bouziane K., Zhou X. L. and Zhou Z., Dalton Trans. 44 (2015) 4526-4532
30. B. Orayech, A. Faik, G. A. Lopez, O. Fabelo and J. M. Igartua (2015) J. Appl. Cryst. 48
31. B. Orayech, I. Urcelay-Olabarria, G. A. Lopez, O. Fabelo, A. Faik and J. M. Igartua, (2015), Dalton Trans., 44, 13867-13880.
32. B. Orayech, L. Ortega-San-Martìn, I. Urcelay-Olabarria, L. Lezama, T. Rojo, Marìa I. Arriortua and J. M. Igartua (2015), Dalton Trans., 44, 13716-13734.